A Kinetic Model for Adsorption and Transfer of Ionic Species at Polarized Liquid|Liquid Interfaces as Studied by Potential Modulated Fluorescence Spectroscopy

ARTICLE *in* THE JOURNAL OF PHYSICAL CHEMISTRY B · OCTOBER 2001

Impact Factor: 3.3 · DOI: 10.1021/jp010732t · Source: OAI

3 AUTHORS:

Hirohisa Nagatani
Kanazawa University
51 PUBLICATIONS **696** CITATIONS
SEE PROFILE

David J. Fermín
University of Bristol
111 PUBLICATIONS **1,841** CITATIONS
SEE PROFILE

Hubert H Girault
École Polytechnique Fédérale de Lausanne
556 PUBLICATIONS **13,980** CITATIONS
SEE PROFILE

A Kinetic Model for Adsorption and Transfer of Ionic Species at Polarized Liquid|Liquid Interfaces as Studied by Potential Modulated Fluorescence Spectroscopy

Hirohisa Nagatani, David J. Fermín, and Hubert H. Girault*

Laboratoire d'Electrochimie, Département de Chimie, Ecole Polytechnique Fédérale de Lausanne, CH-1015 Lausanne, Switzerland

Received: February 26, 2001; In Final Form: June 8, 2001

Fundamental expressions for analyzing potential modulated fluorescence (PMF) responses were derived within the framework of a phenomenological model for adsorption and transfer of ionic species across polarized liquid|liquid interfaces. For small periodic perturbations of the Galvani potential difference, PMF signals can be linearized and the contribution of each process can be uncoupled in the frequency domain. The PMF response for kinetically controlled adsorption is expressed as a semicircle in the complex plane in which the characteristic frequency of maximum imaginary component is proportional to the adsorption and desorption rate constants. Considering that the potential dependence of adsorption exhibits opposite sign whether the process take place from the aqueous or organic phase, the corresponding PMF responses appear in different quadrants of the complex plane. The present model delivers useful diagnostic criteria for analyzing the nature of the various processes contributing to the periodic fluorescence response. The adsorption dynamics of *meso*-tetrakis(*N*-methyl-4-pyridyl)porphyrinato zinc(II) at the water|1,2-dichloroethane interface were evaluated from the frequency dependent PMF responses. Studies performed at various Galvani potential differences clearly confirm that the adsorption can take place at two distinctive planes located at the aqueous and organic sides of the interface. Basic aspects in connection to the nature of the adsorption planes are briefly discussed.

1. Introduction

The molecular structure of interfaces between two immiscible electrolyte solutions (ITIES) remains as a major challenge in the electrochemistry of molecular junctions. Valuable contributions emerging from nonlinear optics,[1−3] total internal reflection (TIR) spectroscopy,[4−7] as well as computer modeling[8−12] have provided different insights into solvent distribution, dynamics, and molecular organization at the interface. For instance, molecular dynamics (MD) simulations have described liquid|liquid interfaces as molecularly sharp junctions roughen by density fluctuations at the picoseconds time scale.[9,10] The average picture derived from these simulations shows a monotonical change of the solvent density over a region of 1 nm, which appears to be consistent with the mixed solvent layer model.[13,14] These results are also in agreement with recent neutron reflectivity study at the water|1,2-dichloroethane interface, where a root-mean-square roughness of the order of 1 nm was estimated.[15]

The structure of the interface has also been probed by surface sensitive spectroscopic techniques. Surface second harmonic generation (SSHG) has been employed for studying the interfacial behavior of ionic species and surfactants.[16−20] Higgins and Corn described the potential dependent adsorption of 2-(*n*-octadecylamino)naphthalene-6-sulfonate at the water|DCE interface by a combination of SSHG and interfacial tension measurements.[21] This pioneering report allowed direct access to surface coverage as a function of the Galvani potential difference. It was obtained that the fraction of the potential drop in the organic side of the interface, from which adsorption takes place, corresponds approximately to 0.7. More recent studies by Piron et al. indicate that a fraction of the applied potential in the aqueous side is close to 0.2 as determined from the adsorption of methyl orange.[19] On the other hand, both studies remarkably contrast with the report by Conboy and Richmond,[18] in which potential dependent SSHG responses showed that the potential drop in the organic side was smaller than 0.1. This result is rather inconsistent with basic descriptions of the potential distribution based on the Gouy−Chapman theory.[22−24]

We have studied the potential dependent adsorption of water-soluble zinc porphyrin and chlorophyll at the water|DCE interface via photocurrent responses originating from the heterogeneous quenching of the excited state,[25−28] as well as potential modulated fluorescence (PMF) spectroscopy[29] and SSHG.[30] The photoelectrochemical and optical responses obtained under TIR employing linearly polarized light indicated that several porphyrin derivatives are specifically adsorbed at the interface with a preferential molecular orientation.[27,29] The basic principle of PMF spectroscopy relies on the measurement of the ac fluorescence associated with a sinusoidal potential perturbation. Because the coverage of *meso*-tetrakis(*N*-methyl-4-pyridyl)porphyrinato zinc(II) ($ZnTMPyP^{4+}$) and *meso*-tetrakis-(4-sulfonatophenyl)porphyrinato zinc(II) ($ZnTPPS^{4-}$) are dependent on the applied Galvani potential difference, the contribution from the adsorbed species to the fluorescence can be simply determined by lock-in detection of the ac spectroscopic responses. This powerful yet simple approach allowed resolving the electrochemical features in connection to adsorption and transfer of the ionic porphyrins. In the present paper, we formulate a theoretical framework for PMF responses involving a parallel scheme for adsorption and transfer of ionic species. The basic PMF responses will be developed for a system in which adsorption planes can be located at either side of the interface and the surface coverage is determined by the bulk concentration and the Galvani potential difference. As postulated in a previous work,[29] the difference in the potential dependence for the adsorption of ionic species from the aqueous or the organic phase introduces a clear change in the phase shift of

10.1021/jp010732t CCC: $20.00
Published on Web 09/06/2001

SCHEME 1: Simplified Representation of the Interfacial Structure and Adsorption Processes[a]

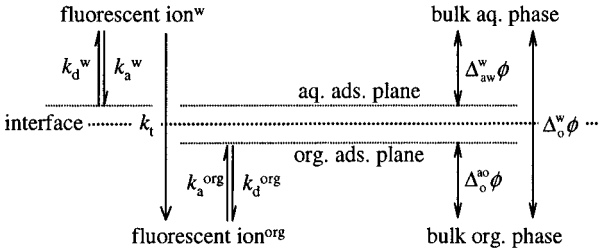

[a] Two adsorption planes are defined at either side of the interface. the potential drop between each adsorption plane and the respective bulk phases determines the adsorption dynamics.

the PMF responses. It is also shown that the potential dependence of the PMF responses can also provide information on the fraction of the potential drop between the bulk phase and the adsorption planes. Furthermore, the frequency dependence of the PMF responses allows accessing the dynamics of adsorption and transfer processes. Simple diagnostic criteria are given for elucidating the adsorption properties of ionic species based on PMF spectroscopy.

2. Theoretical Section

2.1. Langmuir Adsorption Model. The distribution of the probing ion across the interface as a function of the Galvani potential difference can be approached in a simplified fashion by uncoupling the adsorption and transfer processes as depicted in Scheme 1. This assumption allows treating the contribution from both processes to the PMF responses separately with a common steady state boundary condition established by the Nernst equation for ion transfer. The presence of two adsorption planes has been phenomenologically demonstrated by a previous PMF analysis at the water|DCE interface in the presence of ZnTMPyP.[29] In principle, this representation could be related to the modified Verwey−Niessen model for the electrical double layer at polarized liquid|liquid interfaces.[31] The adsorption plane can be regarded as the corresponding inner Helmholtz plane associated with the specific adsorption of the molecule. However, this description should be considered cautiously as MD simulations have clearly shown that the solvent distribution across the interface differs rather significantly from those obtained for metal|electrolyte junctions.[9] The nature of the adsorption plane could be related to a region where the adsorbed species is stabilized by inhomogeneous solvent interactions. From this point of view, the adsorption planes can be defined in terms of the specific solvation properties of the ionic species without involving controversial concepts such as ion-free compact layer or mixed solvent layer.[31] As described in Scheme 1, the present model ignores the contribution to the ion transfer by the preadsorbed species in order to simplify the analysis of the experimental data. Further along the discussion, it is shown that this approach is applicable to several cases in which either adsorption or ion transfer could be the rate-determining step.

Assuming that lateral interaction between adsorbed species as well as the interaction across the two adsorption planes are negligible, the change in surface coverage (θ) for both the aqueous and organic adsorption process can be described by the following differential equation:

$$\frac{d\theta}{dt} = k_a c_0(1-\theta) - k_d\theta \tag{1}$$

where c_0 is the bulk concentration of the adsorbed species and k_a and k_d are the adsorption and desorption rate constants. The adsorption rate is determined by the bulk concentration and the number of adsorption sites, while the desorption rate is proportional to the surface excess. Considering that the distribution of the adsorbed species is affected by the Galvani potential difference ($\Delta_o^w\phi$),[32] the corresponding rate constants for adsorption and desorption can be expressed as function of the potential difference between the bulk and adsorption plane ($\Delta_{aw}^w\phi$ and $\Delta_o^{ao}\phi$) as

$$k_a^w = k_a^{w\circ}\exp\left[\frac{\alpha^w zF}{RT}\Delta_{aw}^w\phi\right] \tag{2}$$

$$k_d^w = k_d^{w\circ}\exp\left[\frac{(\alpha^w-1)zF}{RT}\Delta_{aw}^w\phi\right] \tag{3}$$

$$k_a^{org} = k_a^{org\circ}\exp\left[-\frac{\alpha^{org} zF}{RT}\Delta_o^{ao}\phi\right] \tag{4}$$

$$k_d^{org} = k_d^{org\circ}\exp\left[-\frac{(\alpha^{org}-1)zF}{RT}\Delta_o^{ao}\phi\right] \tag{5}$$

where superscripts "w" and "org" refer to the adsorption from the aqueous and organic phases and the parameter α corresponds to the fraction of the potential drop in a given electrolyte phase operating on the dynamics of adsorption. The parameter α can be regarded as an overall transfer coefficient for the adsorption process. This parameter can adopt any value between 0 and 1.

The potential drop between the bulk phase and the corresponding adsorption plane is a rather difficult parameter to evaluate experimentally in the case of highly charged ionic species. The previous studies by SSHG technique[19−21] have been focused on monovalent amphiphilic species, where a potential drop can be physically defined between the bulk of each phase and the liquid|liquid interface. This approach allows expressing the corresponding potential drop by an adjustable parameter b. In the case of water-soluble zinc porphyrin such as ZnTMPyP, two adsorption planes can be distinguished from PMF measurements, thus the potential drop acting on the adsorption step should be extended to

$$\Delta_{aw}^w\phi = b^w\Delta_o^w\phi \tag{6}$$

$$\Delta_o^{ao}\phi = b^{org}\Delta_o^w\phi \tag{7}$$

where the relationship between b^w and b^{org} is determined by the potential distribution across the two adsorption planes. For instance, considering that $\Delta_{aw}^{ao}\phi$ is negligible small, the expression is simplified to the case where

$$b^w + b^{org} = 1 \tag{8}$$

Consequently $\Delta_{aw}^w\phi = b^w\Delta_o^w\phi$ and $\Delta_o^{ao}\phi = (1-b^w)\Delta_o^w\phi$. However, in the absence of a clear knowledge of the location of the adsorption planes, the assumption given by eq 8 cannot be established a priori.

Equations 2−5 also feature a preexponential factor that defines the adsorption and desorption rate constants in the absence of a potential drop between the bulk and the adsorption planes. Assuming that the specific adsorption does not affect substantially the potential distribution across the interface, i.e., low coverage limit, the parameters k_a° and k_d° correspond to the adsorption and desorption rate constants at the potential of zero charge.

In the steady-state condition, the potential dependence of the surface coverage at the aqueous (θ_0^w) and organic adsorption planes (θ_0^{org}) can be estimated from eqs 1−8,

$$\theta_0^w = \frac{c_0^w \exp[(b^w z F \Delta_o^w\phi - \Delta G_a^{w\circ})/RT]}{c^o + c_0^w \exp[(b^w z F \Delta_o^w\phi - \Delta G_a^{w\circ})/RT]} \quad (9)$$

$$\theta_0^{org} = \frac{c_0^{org} \exp[(-b^{org} z F \Delta_o^w\phi - \Delta G_a^{org\circ})/RT]}{c^\circ + c_0^{org} \exp[(-b^{org} z F \Delta_o^w\phi - \Delta G_a^{org\circ})/RT]} \quad (10)$$

where

$$\Delta G_a^\circ = -RT \ln\left(\frac{k_a^\circ c^\circ}{k_d^\circ}\right) \quad (11)$$

The Langmuir isotherm defined as eqs 9 and 10 have been employed for various adsorption systems as function of the Galvani potential difference at polarized ITIES.[19,21,26] Equations 9 and 10 are consistent with the generalized Frumkin isotherm for liquid|liquid interfaces derived by Markin and Volkov,[33] considering negligible lateral interaction between adsorbed species.

The boundary condition that connects the adsorption processes in both planes is given by the Nernst equation,[32]

$$\Delta_o^w\phi = \Delta_o^w\phi^{\circ\prime} + \frac{RT}{zF}\ln\frac{c_0^{org}}{c_0^w} \quad (12)$$

where $\Delta_o^w\phi^{\circ\prime}$ corresponds to the formal transfer potential. The potential dependence of the surface coverage at the aqueous side as obtained from eqs 2−12 is shown in Figure 1. It is observed that the surface coverage increases as the potential is increased until reaching a maximum. The decrease in the coverage at more positive potentials is associated with a decrease in the equilibrium concentration of the adsorbed species in bulk water due to the transfer to the organic phase. The potential dependence of the surface coverage is clearly affected by the potential distribution across the interface as well as the effective charge of the adsorbed species. Because the parameter b^w and z are convoluted in eq 9, it is difficult to separate their contributions from the experimental point of view in cases where the interfacial ion-pairing can take place. Another important aspect in connection to eq 9 is that, in the case of strongly adsorbed species, i.e., very negative $\Delta G_a^{w\circ}$, and low values for the parameter $b^w z$, the potential dependence of the adsorption could be very weak and saturation is observed at potentials prior to the ion transfer. In the case that the potential drop between adsorption planes is negligible, i.e., eq 8, the potential dependence of θ_0^w appears identical to θ_0^{org} for the conditions shown in Figure 1. However, if eq 8 is not valid, a stronger potential dependence for the surface coverage at the organic side is expected in comparison to the aqueous side, due to the lower dielectric constant for the organic phase which implies that $b^{org} \geq 0.5$.

2.2. Frequency Dependent Fluorescence Associated with Kinetically Controlled Adsorption Processes. The superimposition of a periodic potential perturbation to the Galvani potential difference introduces an ac component of the surface coverage which phase is determined by the frequency and the adsorption and desorption rates. In present system, the applied potential is described as

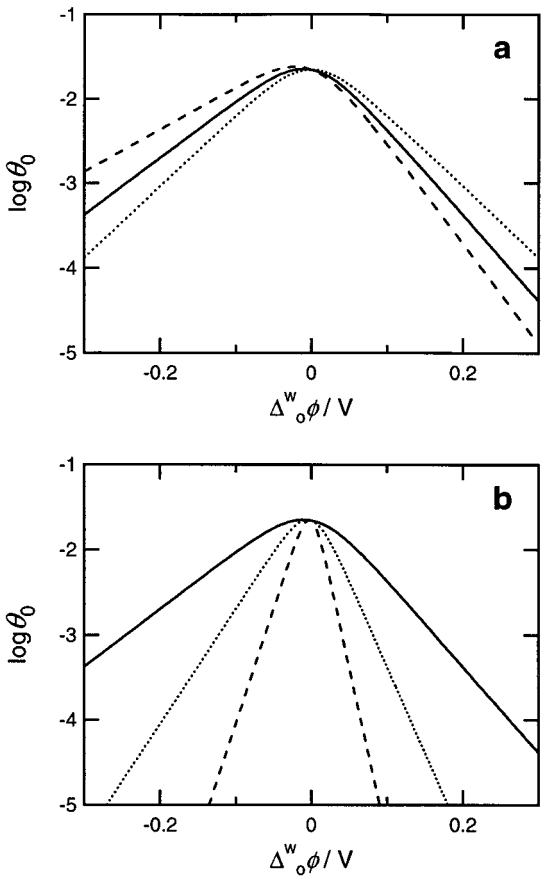

Figure 1. Potential dependent surface coverage calculated from eqs 9−12. **(a)** The potential distribution dependence. b^w and b^{org} were taken as 0.5 and 0.5 (dotted line), 0.4 and 0.6 (solid line), 0.3 and 0.7 (dashed line), respectively. z of the adsorbed species was +1. **(b)** Effects of the charge number. z, was taken as +1 (solid line), +2 (dotted line) and +4 (dashed line), respectively. b^w and b^{org} were 0.4 and 0.6. The values for c_0, $\Delta_o^w\phi^{\circ\prime}$, and ΔG_a° were taken as 1×10^{-8} mol cm^{-3}, 0 V, and −38 kJ mol^{-1}.

$$\Delta_o^w\phi = \Delta_o^w\phi_{dc} + \Delta_o^w\phi_{ac} = \Delta_o^w\phi_0 + \Delta_o^w\phi_1 \exp(i\omega t) \quad (13)$$

then the surface coverage is given by

$$\theta = \theta_{dc} + \theta_{ac} = \theta_0 + \theta_1 \exp(i\omega t) \quad (14)$$

where ω is the angular frequency and the subscripts 0 and 1 correspond to the steady state and frequency dependent components. For small amplitudes of the potential modulation, the frequency dependent components of the adsorption and desorption rate constants can be linearized as follows:

$$k_{a,1}^w = k_{a,0}^w \frac{\alpha^w b^w z F}{RT}\Delta_o^w\phi_1 \quad (15)$$

$$k_{d,1}^w = k_{d,0}^w \frac{(\alpha^w - 1) b^w z F}{RT}\Delta_o^w\phi_1 \quad (16)$$

$$k_{a,1}^{org} = -k_{a,0}^{org} \frac{\alpha^{org} b^{org} z F}{RT}\Delta_o^w\phi_1 \quad (17)$$

$$k_{d,1}^{org} = -k_{d,0}^{org} \frac{(\alpha^{org} - 1) b^{org} z F}{RT}\Delta_o^w\phi_1 \quad (18)$$

It follows that the frequency dependent surface coverage in both phases can be derived from eqs 1, 13−18 as

$$\theta_1^{w} = \frac{b^{w} zF}{RT}\left[\frac{\Delta_o^{w}\phi_1(k_{a,0}^{w}\alpha^{w}c_0^{w}(1-\theta_0^{w}) - k_{d,0}^{w}(\alpha^{w}-1)\theta_0^{w})}{k_{a,0}^{w}\, c_0^{w} + k_{d,0}^{w} + i\omega}\right] \quad (19)$$

$$\theta_1^{org} = -\frac{b^{org} zF}{RT}\left[\frac{\Delta_o^{w}\phi_1(k_{a,0}^{org}\alpha^{org}c_0^{org}(1-\theta_0^{org}) - k_{d,0}^{org}(\alpha^{org}-1)\theta_0^{org})}{k_{a,0}^{org}\, c_0^{org} + k_{d,0}^{org} + i\omega}\right] \quad (20)$$

Finally, the frequency dependent fluorescence signal associated with the adsorption process can be derived from eqs 19 and 20 taking into account the molar absorptivity ϵ, the fluorescence quantum yield Φ, and the excitation photon flux I_{exc}.

$$\Delta F_a^{w} = \frac{2.303\epsilon^{w}\Phi^{w}I_{exc}^{w}\Gamma_s^{w}Sb^{w}zF}{RT}\left[\frac{\Delta_o^{w}\phi_1(k_{a,0}^{w}\, c_0^{w}\alpha^{w}(1-\theta_0^{w}) - k_{d,0}^{w}(\alpha^{w}-1)\theta_0^{w})}{k_{a,0}^{w}\, c_0^{w} + k_{d,0}^{w} + i\omega}\right] \quad (21)$$

$$\Delta F_a^{org} = -\frac{2.303\epsilon^{org}\Phi^{org}I_{exc}^{org}\Gamma_s^{org}Sb^{org}zF}{RT}\left[\frac{\Delta_o^{w}\phi_1(k_{a,0}^{org}\, c_0^{org}\alpha^{org}(1-\theta_0^{org}) - k_{d,0}^{org}(\alpha^{org}-1)\theta_0^{org})}{k_{a,0}^{org}\, c_0^{org} + k_{d,0}^{org} + i\omega}\right] \quad (22)$$

where S is the illuminated interfacial area and Γ_s is the saturated interfacial concentration. It should also be considered that the illumination under a TIR condition introduces complications concerning the effective photon flux at each adsorption plane. For the water|DCE system, the excitation beam passed through the organic phase; therefore, the effective photon flux across the organic adsorption plane (I_{exc}^{org}) can be easily quantified assuming that no absorption take place in the bulk organic phase. On the other hand, the excitation at the aqueous adsorption plane is formally associated with the evanescent wave propagating into the aqueous phase. The light intensity drops exponentially away from the interface, consequently the aqueous adsorption plane must be located no further than tens of nm from the reflection plane in order to be sensitive to visible illumination in TIR. (e.g., the penetration depth is ca. 72 nm in present experimental condition.) Furthermore, the molar absorptivity and the fluorescence quantum yield can also be dependent on the solvent properties.

For the adsorption at the aqueous side, the real and imaginary components of the frequency dependent fluorescence can be evaluated as

$$\Delta F_{a,re}^{w} = \frac{2.303\epsilon^{w}\Phi^{w}I_{exc}^{w}\Gamma_s^{w}Sb^{w}zF}{RT}\left[\frac{\Delta_o^{w}\phi_1(k_{a,0}^{w}\alpha^{w}c_0^{w}(1-\theta_0^{w}) - k_{d,0}^{w}(\alpha^{w}-1)\theta_0^{w})(k_{a,0}^{w}\, c_0^{w} + k_{d,0}^{w})}{(k_{a,0}^{w}\, c_0^{w} + k_{d,0}^{w})^2 + \omega^2}\right] \quad (23)$$

$$\Delta F_{a,im}^{w} = \frac{2.303\epsilon^{w}\Phi^{w}I_{exc}^{w}\Gamma_s^{w}Sb^{w}zF}{RT}\left[\frac{\Delta_o^{w}\phi_1(k_{a,0}^{w}\alpha^{w}c_0^{w}(1-\theta_0^{w}) - k_{d,0}^{w}(\alpha^{w}-1)\theta_0^{w})\omega}{(k_{a,0}^{w}\, c_0^{w} + k_{d,0}^{w})^2 + \omega^2}\right] \quad (24)$$

The corresponding expressions for the adsorption from the organic side are analogous to eqs 23 and 24 with the appropriate reversal of sign. The potential dependence of the real and imaginary components of ΔF is displayed in Figure 2. The value of α was taken as 0.5 for both phases. In the case of a cationic species, the maximum PMF response for the adsorption at the aqueous side appears at potentials less positive than the formal transfer potential (Figure 2a). Contrastingly, the PMF response for adsorption at the organic side is maximized at potentials more positive than $\Delta_o^{w}\phi^{o\prime}$ (Figure 2b). Both processes are clearly distinguishable due to the 180° phase shift arising from the difference in the sign between eqs 21 and 22. The width and height of the adsorption peak depends strongly on the potential distribution as well as the charge number of ionic species (Figure 2c,d).

For kinetically controlled adsorption, the complex representation of PMF is described as a semicircle as shown in Figure 3. The frequency of maximum imaginary component is determined by the value of the adsorption and desorption rate constants. Numerical simulations in Figure 3 were performed with rate constants of the same order as the experimental values discussed in further sections. As mentioned earlier, the position of the PMF complex plane can be considered as a criterion for determining the relative location of the adsorption plane.

2.3. Basic PMF Responses Involving Transfer and Adsorption Processes. The simple approximation employed in this model allows incorporating the PMF responses associated with a quasi-reversible ion transfer. In a previous paper, it was derived that the frequency dependent fluorescence response ΔF_t is effectively 90° phase shifted with respect to the Faradaic ac current I_f:[29,34]

$$\Delta F_t = \frac{4.606\epsilon\Phi I_{exc}}{i\omega|z|F\cos\psi} I_{f,1} \quad (25)$$

where ψ is the angle of incidence of the excitation beam. The magnitude of the faradaic ac current $I_{f,1}$ can be estimated from the ion transfer impedance Z_f

$$I_{f,1} = \frac{\Delta_o^{w}\phi_1}{Z_f} = \frac{\Delta_o^{w}\phi_1}{R_{ct} + (1-i)\sigma\omega^{-0.5}} \quad (26)$$

where R_{ct} and σ are the charge-transfer resistance and the Warburg term, respectively. Considering that the ion transfer occurs from the water to the organic phase, the impedance components can be expressed in terms of the ion transfer rate constant (k_t) and the diffusion coefficient (D^{w}),[35−38]

$$R_{ct} = \frac{RT}{z^2F^2Sk_tc_0^{w}} \quad (27)$$

$$\sigma^{w} = \frac{4RT\cosh^2(zF(\Delta_o^{w}\phi - \Delta_o^{w}\phi^{o\prime})/2RT)}{z^2F^2Sc_0^{w}(2D^{w})^{0.5}} \quad (28)$$

Finally, the real and imaginary components of the PMF response for the ion transfer are described as

$$\Delta F_{t,re} = \frac{4.606\epsilon^{org}\Phi^{org}I_{exc}^{org}}{|z|F\cos\psi}\left[\frac{\Delta_o^{w}\phi_1\sigma^{w}\omega^{-1.5}}{(R_{ct}+\sigma^{w}\omega^{-0.5})^2 + (\sigma^{w}\omega^{-0.5})^2}\right] \quad (29)$$

$$\Delta F_{t,im} = -\frac{4.606\epsilon^{org}\Phi^{org}I_{exc}^{org}}{|z|F\cos\psi}\left[\frac{\Delta_o^{w}\phi_1(R_{ct}+\sigma^{w}\omega^{-0.5})\omega^{-1}}{(R_{ct}+\sigma^{w}\omega^{-0.5})^2 + (\sigma^{w}\omega^{-0.5})^2}\right] \quad (30)$$

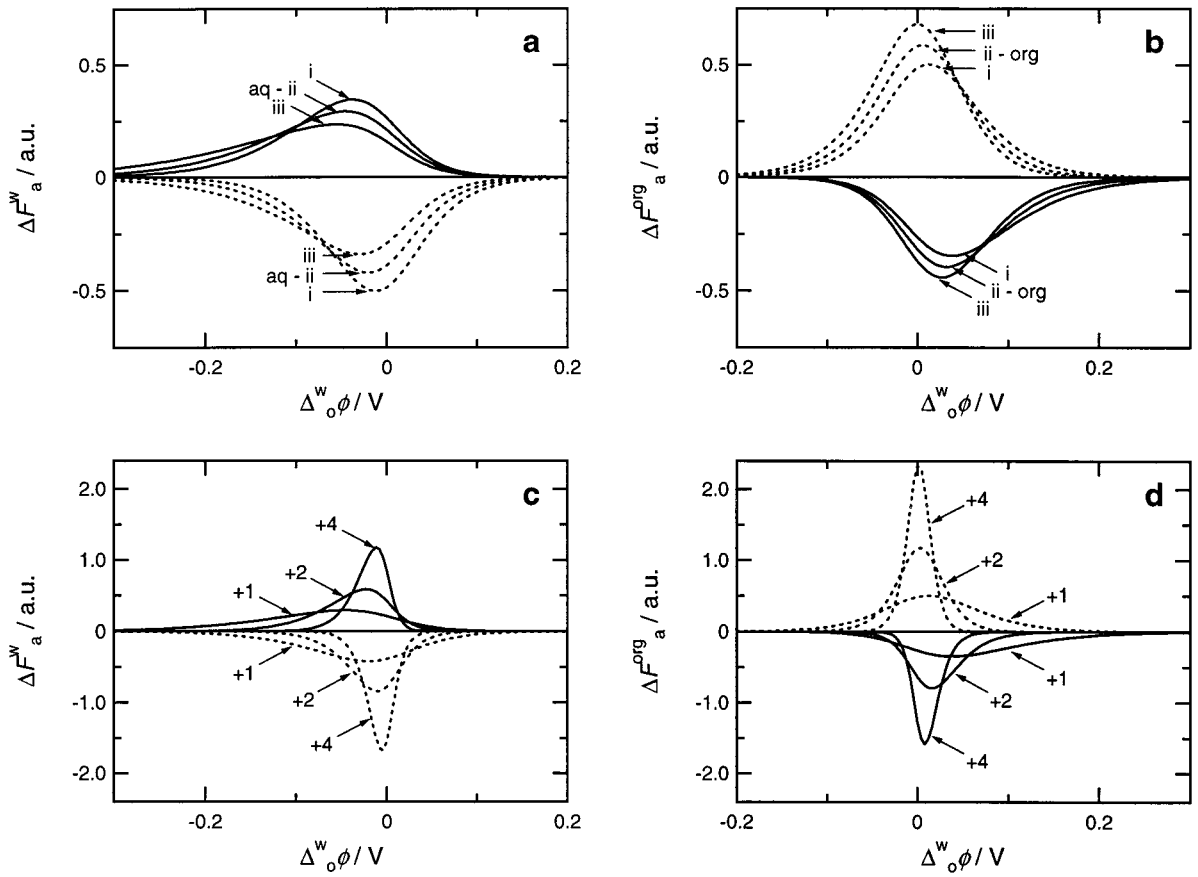

Figure 2. Potential dependence of the PMF responses for a kinetically controlled adsorption from **(**a, c**)** the aqueous and **(**b, d**)** organic sides. **(**a, b**)** The potential distribution dependence. b^w and b^{org} were taken as (i) 0.5 and 0.5, (ii) 0.4 and 0.6, (iii) 0.3 and 0.7, respectively. z of the adsorbed species was +1. **(**c, d**)** Effects of the charge number. z was changed from +1 to +4. The solid and dashed lines relate the real and imaginary components calculated from eqs 23 and 24. The frequency of potential modulation, c_0, $\Delta^w_o\phi^\circ$, and ΔG°_a were 3 Hz, 1×10^{-8} mol cm^{-3}, 0 V, and −38 kJ mol^{-1}, respectively.

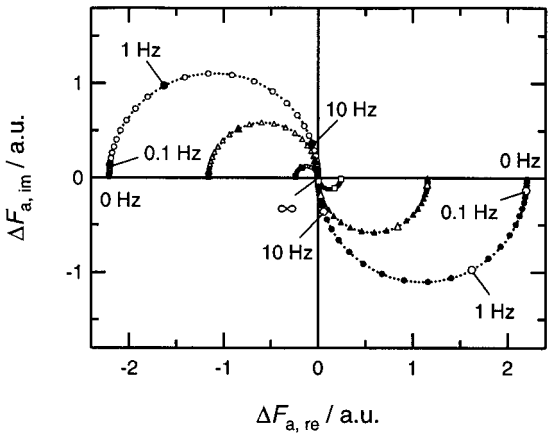

Figure 3. Frequency dependence of the PMF responses for a kinetically controlled adsorption process. The closed and open symbols depict the adsorption at the aqueous and organic sides of the interface. The circle, triangle, and square relate to $k_{a,0} = 1 \times 10^8$, 5×10^7 and 1×10^7 dm^3 mol^{-1} s^{-1}, respectively. $k_{d,0}$ was fixed to 10 s^{-1}.

The complex representation for various ion transfer rate constants is illustrated in Figure 4. Neglecting any attenuation of the amplitude of the ac potential at high frequencies,[38] the ion transfer rate constant can be accessed directly from the frequency dependence of the PMF responses within the range exemplified in Figure 4. For a transfer rate constant above 0.1 cm s^{-1}, the PMF responses appear insensitive to the charge-transfer resistance.

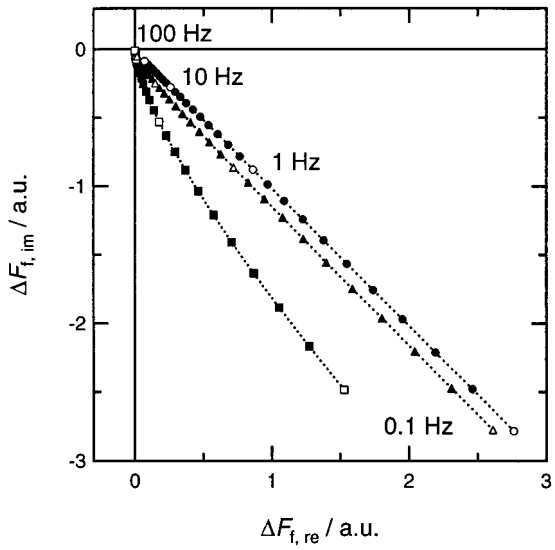

Figure 4. Complex representation of the PMF for a quasi-reversible transfer of a monocation. The circle, triangle and square relate to k_t = 0.1, 0.01 and 0.001 cm s^{-1}, respectively. D^w was taken as 5×10^{-6} cm^2 s^{-1}.

The PMF responses for ion transferring from water to DCE can be described by eqs 29 and 30. In the case that adsorption takes place close to the transfer potential, the frequency dependent fluorescence would involve a convolution of the ac response associated with the change in surface coverage and

TABLE 1: Theoretical Equations for PMF Responses

adsorption process from the aqueous phase[a]		
ac fluorescence	$\Delta F_a^w = \frac{2.303\epsilon^w \Phi^w I_{exc}^w \Gamma_s^w S b^w zF}{RT}\left[\frac{\Delta_o^w \phi_1 (k_{a,0}^w c_0^w \alpha^w (1-\theta_0^w) - k_{d,0}^w (\alpha^w - 1)\theta_0^w)}{k_{a,0}^w c_0^w + k_{d,0}^w + i\omega}\right]$	(eq 21)
real part	$\Delta F_{a,re}^w = \frac{2.303\epsilon^w \Phi^w I_{exc}^w \Gamma_s^w S b^w zF}{RT}\left[\frac{\Delta_o^w \phi_1 (k_{a,0}^w \alpha^w c_0^w (1-\theta_0^w) - k_{d,0}^w (\alpha^w - 1)\theta_0^w)(k_{a,0}^w c_0^w + k_{d,0}^w)}{(k_{a,0}^w c_0^w + k_{d,0}^w)^2 + \omega^2}\right]$	(eq 23)
imaginary part	$\Delta F_{a,im}^w = -\frac{2.303\epsilon^w \Phi^w I_{exc}^w \Gamma_s^w S b^w zF}{RT}\left[\frac{\Delta_o^w \phi_1 (k_{a,0}^w \alpha^w c_0^w (1-\theta_0^w) - k_{d,0}^w (\alpha^w - 1)\theta_0^w)\omega}{(k_{a,0}^w c_0^w + k_{d,0}^w)^2 + \omega^2}\right]$	(eq 24)
quasi-reversible ion transfer process		
ac fluorescence	$\Delta F_t = \frac{4.606\epsilon \Phi I_{exc}}{i\omega |z| F \cos\psi} I_{f,1}$	(eq 25)
real part	$\Delta F_{t,re} = \frac{4.606\epsilon^{org} \Phi^{org} I_{exc}^{org}}{|z| F \cos\psi}\left[\frac{\Delta_o^w \phi_1 \sigma^w \omega^{-1.5}}{(R_{ct} + \sigma^w \omega^{-0.5})^2 + (\sigma^w \omega^{-0.5})^2}\right]$	(eq 29)
imaginary part	$\Delta F_{t,im} = -\frac{4.606\epsilon^{org} \Phi^{org} I_{exc}^{org}}{|z| F \cos\psi}\left[\frac{\Delta_o^w \phi_1 (R_{ct} + \sigma^w \omega^{-0.5})\omega^{-1}}{(R_{ct} + \sigma^w \omega^{-0.5})^2 + (\sigma^w \omega^{-0.5})^2}\right]$	(eq 30)

[a] The appropriate reverse sign is applied to the adsorption process from the organic phase.

the diffusion layer concentration. The contribution of each process at a given frequency will depend not only on the fluorescence efficiency but also on the corresponding dynamics. For instance, while ΔF_t increases as the frequency is decreased with a phase shift close to $-45°$ with respect to the ac potential, the dynamic adsorption responses approach 0° phase shift. On the other hand, if the adsorption processes are rather fast, the PMF responses associated with the adsorption will provide the larger contribution at a higher frequency. The main equations describing the PMF responses for kinetically controlled adsorption and quasi-reversible ion transfer are summarized in Table 1.

Within the framework of parallel and independent adsorption and transfer processes, the PMF response can simply be expressed as the sum of two contributions:

$$\Delta F = \Delta F_a + \Delta F_t \tag{31}$$

This parallel scheme can be compared to the Laitinen and Randles model for impedance responses at metal electrodes in the presence of specific adsorption.[39] This model accounts for deviations of the typical Randles behavior by incorporating a resistance and a capacitance in parallel to the faradaic elements. These extra elements are associated with the charge-transfer resistance and the perturbation of the interfacial charge in connection to the adsorbed species. More sophisticated models were also proposed by Senda and Delahay[40] and Sluyters-Rehbach et al.,[41] where different equivalent circuits and boundary conditions were considered for describing the faradaic and nonfaradaic contributions to the impedance. Later, Delahay demonstrated that faradaic and nonfaradaic components of transient electrochemical responses cannot be separated a priori due to interfacial charge separation phenomena without flow of external current.[42] In principle, one of the major advantages of employing techniques such as PMF spectroscopy is that no additional treatment is required for uncoupling the periodic changes in concentration of the fluorescent species from other elements such as the interfacial capacitance.

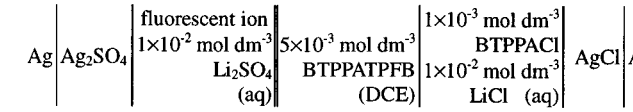

Figure 5. Schematic representation of the electrochemical cell.

Although the frequency dependent PMF responses have been explicitly derived by kinetically controlled adsorption, the same approach can be extended for fast adsorption and desorption processes. If we consider a diffusion-controlled adsorption, the frequency dependent diffusion profile will have a similar form than for reversible ion transfer processes. In this case, eqs 27−30 are also applicable upon replacing $\Delta_o^w \phi^{o\prime}$ and $\Delta_o^w \phi$ by $-\Delta G_a/zF$ and $b\Delta_o^w \phi$, respectively.

The proposed kinetic model will be applied to the PMF responses at the water|DCE interface in the presence of a cation, $Ru(bpy)_3^{2+}$ or $ZnTMPyP^{4+}$. In previous studies,[29] it was concluded that the transfer of $Ru(bpy)_3^{2+}$ takes place in the absence of the adsorption process and it is expected that the PMF response can be determined by eqs 29 and 30. On the other hand, ZnTMPyP appears to be adsorbed at both sides of the interface at the potentials close to the formal transfer potential.

3. Experimental Section

Reagents. The fluorescent species, *meso*-tetrakis(*N*-methyl-4-pyridyl)porphyrinato zinc(II) tetratosylate ($ZnTMPyP(tos)_4$) and tris(2,2′-bipyridyl)ruthenium(II) dichloride ($Ru(bpy)_3Cl_2$), were purchased from Porphyrin Products and Aldrich, respectively. The composition of the electrolyte solutions is schematically shown in Figure 5. The supporting electrolyte was bis(triphenylphosphoranylidene)ammonium tetrakis(pentafluorophenyl)borate (BTPPATPFB)[25] for the 1,2-dichloroethane (DCE) phase and Lithium sulfate for the aqueous phase, respectively. 7,7,8,8-Tetracyanoquinodimethane (TCNQ) was used as a fluorescence quencher in the organic phase. All of

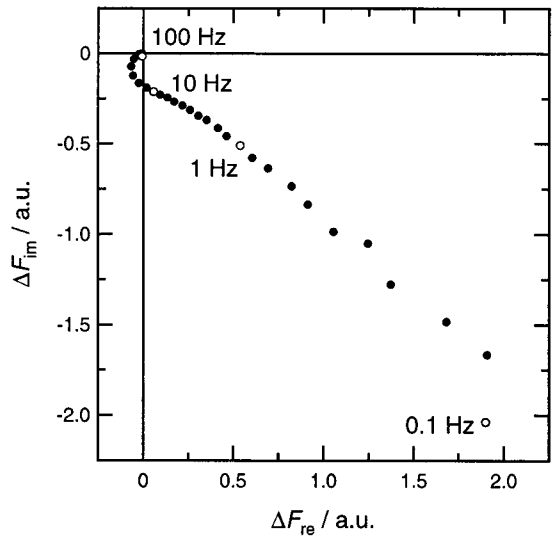

Figure 6. Complex representation of the PMF responses for the transfer of $Ru(bpy)_3^{2+}$ at −0.10 V. The concentration of $Ru(bpy)_3^{2+}$ was 2.5×10^{-5} mol dm^{-3}. The frequency of potential modulation was varied from 0.1 to 100 Hz with amplitude of 25 mV.

the reagents were analytical grade or higher. The Galvani potential difference was estimated by taking the formal transfer potentials of tetramethylammonium as 0.160 V and tetrapropylammonium as −0.093 V. The aqueous solutions were prepared with the purified water by a Milli-Q system (Millipore Milli-Q.185).

Apparatus. A three compartments spectroelectrochemical cell described elsewhere was used for all measurements.[29] The surface area was 0.22 cm^2. The illumination in TIR was performed by a cw He−Cd laser of 132 mW at 442 nm (OmNichrome Model 2074-M-A03). The laser power was attenuated to approximately 20 mW in order to avoid bleaching of the aqueous phase. The angle of incidence of the excitation beam was ca. 80°, and the fluorescence was collected perpendicularly to the interface by a liquid light guide fitted to a photomultiplier tube. A GG475 filter was employed for cutting off the excitation wavelength. Further detail of the optical set up has been reported previously.[29] Platinum wires were used as counter-electrodes in both phases and the interface was polarized by a custom-made four-electrode potentiostat with a waveform generator (Hi-Tek Instruments PPR1). The ac modulated fluorescence signal was analyzed by a lock-in amplifier (Stanford Research Systems SR830) for potential dependence measurements at a single frequency, while a frequency response analyzer (Solartron 1250) was employed for frequency dependence measurements.

4. Results and Discussion

4.1. Frequency Dependence Measurements for the Transfer of $Ru(bpy)_3^{2+}$. As described in a previous paper,[29] the PMF signal for the transfer of $Ru(bpy)_3^{2+}$ from water to DCE features a bell-shaped response centered at the formal transfer potential. This behavior coincides with the ac voltammogram under the same conditions, suggesting that no significant adsorption takes place at the interface. The frequency dependent PMF response at the formal transfer potential is displayed in Figure 6. The amplitude of potential modulation was 25 mV and the frequency was varied from 0.1 to 100 Hz. The basic features of the PMF response are similar to those shown in Figure 4, except at high frequencies where the signal appeared in the third quadrant of the complex plane.

The high-frequency features could be associated with an attenuation of the ac potential modulation due to the uncompensated resistance across the reference electrodes. On the conventional equivalent circuit for a liquid|liquid interface, the total impedance (Z_T) is described by[38]

$$Z_T = R_u + \left[i\omega C_{dl} + \frac{1}{R_b} + \frac{1}{R_{ct} + (1 - i)\sigma\omega^{-0.5}} \right]^{-1} \quad (32)$$

where R_u is the uncompensated solution resistance, C_{dl} is the interfacial capacitance and R_b is the supporting electrolyte transfer resistance. Taking into account that the ac potential can be attenuated by a magnitude proportional to the ac current and R_u, the effective potential modulation across the interface can be estimated as

$$\Delta_o^w \phi_1^{eff} = \Delta_o^w \phi_1 \left[1 - \frac{R_u}{Z_T} \right]$$

$$= \Delta_o^w \phi_1 \left[1 - \frac{R_u(1 + i\omega C_{dl} R_b)(R_{ct} + (1 - i)\sigma\omega^{-0.5}) + R_b R_u}{R_u(1 + i\omega C_{dl} R_b)(R_{ct} + (1 - i)\sigma\omega^{-0.5}) + R_b(R_u + R_{ct} + (1 - i)\sigma\omega^{-0.5})} \right] \quad (33)$$

The expression for the PMF response for a quasi-reversible ion transfer (eqs 29 and 30) with the ac potential attenuation are described as follows:

$$\Delta F'_{t,re} = \frac{4.606 \epsilon^{org} \Phi^{org} I_{exc}^{org}}{|z| F \cos\psi} \left[\frac{\Delta_o^w \phi_{1,re}^{eff} \sigma\omega^{w-1.5} + \Delta_o^w \phi_{1,re}^{eff} (R_{ct} + \sigma^w \omega^{-0.5})\omega^{-1}}{(R_{ct} + \sigma^w \omega^{-0.5})^2 + (\sigma^w \omega^{-0.5})^2} \right] \quad (34)$$

$$\Delta F'_{t,im} = -\frac{4.606 \epsilon^{org} \Phi^{org} I_{exc}^{org}}{|z| F \cos\psi} \left[\frac{\Delta_o^w \phi_{1,re}^{eff} (R_{ct} + \sigma^w \omega^{-0.5})\omega^{-1} - \Delta_o^w \phi_{1,im}^{eff} \sigma^w \omega^{-1.5}}{(R_{ct} + \sigma^w \omega^{-0.5})^2 + (\sigma^w \omega^{-0.5})^2} \right] \quad (35)$$

where $\Delta_o^w \phi_{1,re}^{eff}$ and $\Delta_o^w \phi_{1,im}^{eff}$ are the real and imaginary components of the effective potential modulation. Evaluation of eqs 34 and 35 indicates that the effect of the ohmic drop becomes evident at high frequencies. Figure 7 shows numerical simulations of the frequency dependent PMF responses for a divalent cation transfer from water to DCE. The values for k_t, D^w, R_b, and R_u were taken as 0.1 cm s^{-1}, 1×10^{-5} cm^2 s^{-1}, 40 kΩ, and 500 Ω, respectively. For large values of interfacial capacitance and uncompensated solution resistance, the high frequency features appears similarly to those observed experimentally for the $Ru(bpy)_3^{2+}$ system (Figure 6). Comparing the behavior in Figures 4 and 7, it can be concluded that ac potential attenuation can introduce features similar to those expected for slow ion transfer kinetics. Kakiuchi and Takasu exposed similar arguments for kinetics studies of ion transfer by chronofluorometry.[43]

4.2. Dynamic PMF Responses of Adsorption and Transfer of $ZnTMPyP^{4+}$. The potential dependence of PMF responses for the adsorption and transfer of $ZnTMPyP^{4+}$ from water to DCE is displayed in Figure 8. In agreement with previous studies,[29] $ZnTMPyP^{4+}$ exhibits PMF responses at potentials prior and after the formal transfer potential (0.10 V). These features were interpreted in terms of specific adsorption at the aqueous

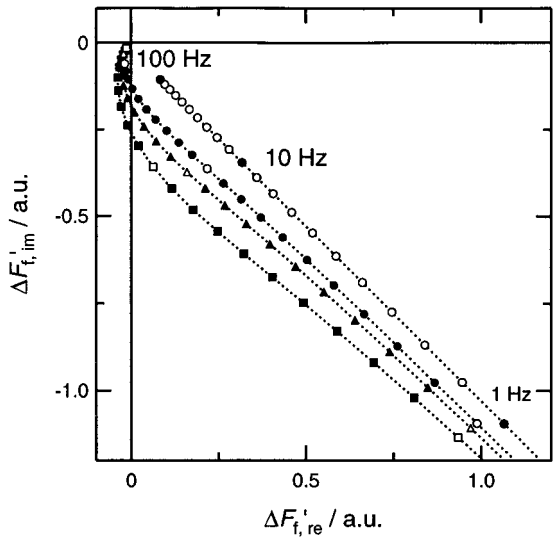

Figure 7. Effects of the ohmic drop on the PMF responses for a quasi-reversible ion transfer. The circle, triangle, and square refer to C_{dl} of 5, 10, and 20 μF. The values of D^w, z, R_u and R_b were taken as 1×10^{-5} cm^2 s^{-1}, +2, 500 Ω, and 40 kΩ, respectively.

and organic sides of the interface. The sharp response in connection to the adsorption at the organic side was observed close to 0.14 V, while the broad response between −0.20 and −0.05 V corresponds to the adsorption at the aqueous side. Considering the positive charge of $ZnTMPyP^{4+}$, the phase shift for the adsorption process at the aqueous and organic sides is consistent with those described by eqs 21−24 (cf. Figure 2). All these features also appear dependent on the frequency of potential modulation as shown in Figure 8a. These results suggest that the dynamics of adsorption and desorption can be affected within the frequency range accessible at potentiostatically controlled liquid|liquid interface.

The nature of the PMF response for adsorption is further confirmed by the effect of the fluorescence quencher, TCNQ, introduced into the organic phase (Figure 8b). The responses at positive potentials were mostly affected by the presence of TCNQ due to the homogeneous electron transfer involving the singlet state of ZnTMPyP. The quenching of the PMF is relatively less effective for the species adsorbed at the aqueous side as the rate of heterogeneous electron transfer is significantly smaller than the rate of intersystem crossing.[26,44] It should also be taken into account that TCNQ exhibits some absorption at the wavelength of excitation, which may account for part of the overall decrease in the PMF amplitude. On the other hand, the effect of the quencher on the PMF response associated with the transfer of $ZnTMPyP^{4+}$ from water to DCE was smaller than expected. As discussed previously, the origin of the ac spectroscopic signal is associated with the modulation of concentration in the interfacial region. The frequency of modulation is orders of magnitude smaller than the homogeneous quenching rate and the PMF response for the transfer should also be substantially reduced in the presence of TCNQ. The reasons behind this unexpected PMF response associated with the porphyrin transfer remain unclear, although it is possible that contribution from adsorption processes at the aqueous side can further extend to this potential region.

In addition to the phase shift, the potential dependence of the adsorption response revealed basic differences between the adsorption at the aqueous and organic sides. The former shows a broader PMF response than the latter, suggesting that the fraction of the Galvani potential difference operating on the organic adsorption process is larger than on the aqueous side (cf. Figure 2). In principle, this result agrees with a simple description of the potential distribution in terms of the modified Verwey-Niessen model, taking into account the higher dielectric constant for the aqueous phase. However, the comparison with

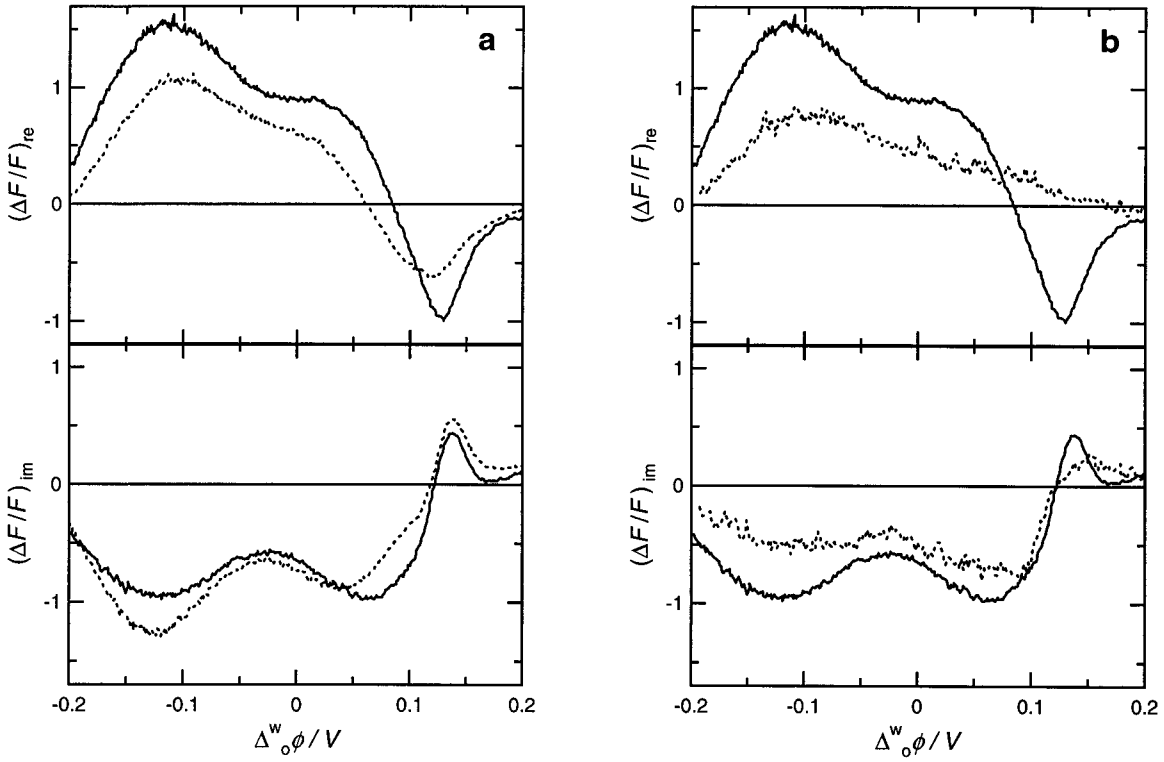

Figure 8. Normalized PMF responses for $ZnTMPyP^{4+}$ system. **(a)** The PMF responses at 3 Hz (solid line) and 6 Hz (dashed line). **(b)** The PMF responses at 3 Hz in the absence (solid line) and presence (dashed line) of 1×10^{-3} mol dm^{-3} TCNQ in DCE. The concentration of $ZnTMPyP^{4+}$ and the amplitude of potential modulation were 2.5×10^{-5} mol dm^{-3} and 10 mV, respectively. The potential sweep rate was 5 mV s^{-1}.

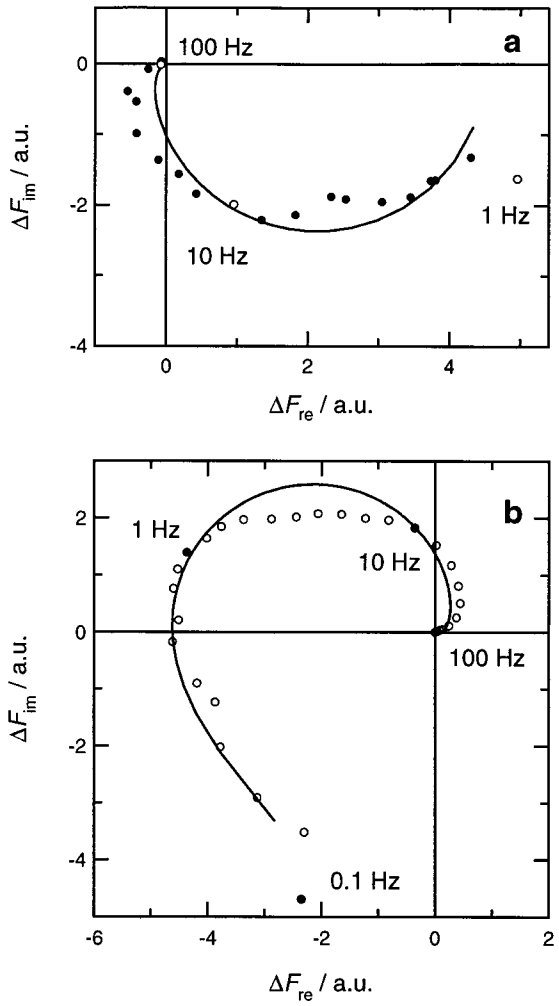

Figure 9. Complex representation of the PMF responses for the $ZnTMPyP^{4+}$ system at **(**a**)** −0.10 and **(b)** 0.14 V. The concentration of $ZnTMPyP^{4+}$ was 2.5×10^{-5} mol dm^{-3}. The amplitude of potential modulation was 25 mV. The solid lines were obtained from the curve fitting with theoretical eqs 36 and 37 for **(**a**)** and eqs 31 and 34−37 for **(**b**)**, respectively. The values of C_{dl}, R_u, and R_b were 5 μF, 350 Ω, and 40 kΩ., respectively.

the numerical simulations in Figures 2c and 2d indicates that the effective charge number of the porphyrin molecule adsorbed at the aqueous side is less than +4. This effect can be associated with interfacial ion-pairing phenomena. For instance, capacitance measurements at the water|DCE interface in the presence of *meso*-tetrakis(4-carboxyphenyl)porphyrinato zinc(II) have shown that specific adsorption can take place in conjunction to interfacial ion pairing.[26]

The dynamics of the adsorption processes at the aqueous and organic sides was investigated by the frequency response analysis of PMF responses at −0.10 and 0.14 V. Representations of the PMF responses in the complex plane are displayed in Figure 9. The appearance of the PMF response in the fourth quadrant for the adsorption at the aqueous side and in the second quadrant for adsorption at the organic side is entirely consistent with the theoretical description illustrated in Figure 3. However, the dynamic responses reveal complex features in which the contribution of other processes within the frequency range from 1 to 100 Hz should be considered. In the case of adsorption at the aqueous side (Figure 9a), the distortion of the semicircular response at high frequencies was interpreted in terms of the attenuation of the ac potential in a fashion similar to the case of $Ru(bpy)_3^{2+}$ (eqs 34 and 35). Consequently, eqs 23 and 24 can be rewritten as

$$\Delta F'_{a,re} = \frac{2.303\epsilon^w \Phi^w I^w_{exc} \Gamma^w_s S b^w z F}{RT} \times \left[\frac{(k^w_{a,0}\, c^w_0 \alpha^w (1-\theta_0) - k^w_{d,0}(\alpha^w - 1)\theta^w_0)(\Delta^w_o\, \phi^{eff}_{1,re}(k^w_{a,0}\, c^w_0 + k^w_{d,0}) + \Delta^w_o\, \phi^{eff}_{1,re}\omega)}{(k^w_{a,0}\, c_0 + k^w_{d,0})^2 + \omega^2}\right] \quad (36)$$

$$\Delta F'_{a,im} = -\frac{2.303\epsilon^w \Phi^w I^w_{exc} \Gamma^w_s S b^w z F}{RT} \times \left[\frac{(k^w_{a,0}\, c^w_0 \alpha^w (1-\theta^w_0) - k^w_{d,0}(\alpha^w - 1)\theta^w_0)(\Delta^w_o\, \phi^{eff}_{1,re}\omega - \Delta^w_o\, \phi^{eff}_{1,im}(k^w_{a,0}\, c^w_0 + k^w_{d,0}))}{(k^w_{a,0}\, c^w_0 + k^w_{d,0})^2 + \omega^2}\right] \quad (37)$$

The solid line in Figure 9a corresponds to a nonlinear least-squares curve fitting with eqs 36 and 37 taking as adjustable parameters $k^w_{a,0}$ and $k^w_{d,0}$ as well as the proportionality factor corresponding to the pre-brackets term in each equation. The values of C_{dl}, R_u, and R_b were estimated from impedance measurements under the same conditions in the absence of $ZnTMPyP^{4+}$. The curve fitting is able to reproduce the basic features obtained experimentally. Although the obtained rate constants include uncertainty arising from the proportionality factor, the values of $k^w_{a,0}$ and $k^w_{d,0}$ could be estimated as the order of 10^7−10^9 cm^3 mol^{-1} s^{-1} and 15−30 s^{-1}, respectively.

The frequency dependence of the PMF response for the adsorption at the organic side (0.14 V) also showed some complex features at low frequencies (Figure 9b). In this case, the adsorption response was convoluted with the ion transfer response taking place within the same potential range. The analysis of these data is complicated by the fact that the volume ratio between the organic and aqueous phases does not allow to effectively employ the boundary condition established by the Nernst equation (eq 12). The experiment displayed in Figure 9b was recorded after imposing a potential of 0.14 V for ca. 1 h. The bulk concentration of the organic phase was estimated colorimetrically. The solid line in Figure 9b corresponds to the PMF expression involving the transfer and adsorption processes given by eqs 31 and 34−37. As the adsorption process occurs at the organic side, the appropriate sign reversal and changes of the proportionality factors were introduced in eqs 36 and 37. The curve fitting was rather insensitive to the charge transfer resistance, indicating that the kinetics of the ion transfer process is effectively controlled by planar diffusion in the aqueous phase. The obtained values of $k^{org}_{a,0}$ and $k^{org}_{d,0}$ are on the order of 10^7−10^8 cm^3 mol^{-1} s^{-1} and 20 s^{-1}. The Gibbs free energy of adsorption can be evaluated from these kinetic parameters and eq 11, in which values between −30 and −40 kJ mol^{-1} for ΔG_a were obtained.

The frequency dependence analysis at 0.14 V was also performed in the presence of the porphyrin salt $(ZnTMPyP^{4+})$-$(TPFB^-)_4$ initially located in the organic solution. These measurements are rather difficult as the ac response is convoluted with a large dc fluorescence signal generated throughout the organic phase. Nevertheless, this approach allows establishing more effectively the equilibrium between bulk concentration and the adsorption plane in the organic side. As exemplified in Figure 10, the basic features of the PMF responses are similar to those observed in Figure 9b. Distortions of the semicircular response at high frequencies are also observed which could not be reproduced by eqs 36 and 37. Despite these nonideal features, the rate constants obtained from this analysis were compatible to those obtained from the analysis of Figure 9b.

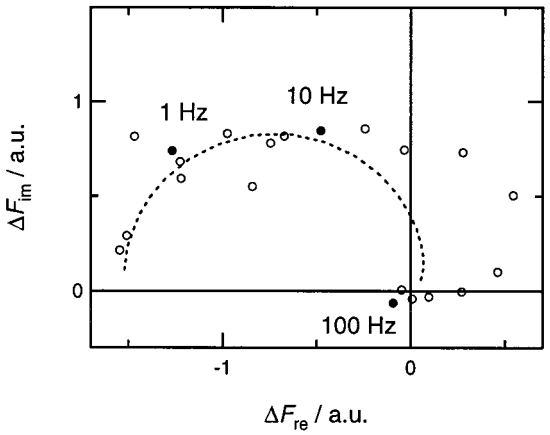

Figure 10. Complex representation of the PMF responses in the presence of $(ZnTMPyP^{4+})(TPFB^{-})_4$ in DCE. The concentration of $(ZnTMPyP^{4+})(TPFB^{-})_4$ was 2.5×10^{-6} mol dm^{-3}. The dc bias and the amplitude of potential modulation were 0.14 V and 25 mV.

The rationalization of the phenomenological rate constants obtained from the analysis illustrated in Figures 9 and 10 requires some extra approximations in order to uncouple the effect of the applied potential. Assuming that the adsorption of the ionic species does not bring about substantial changes in the potential distribution, the parameters k_a° and k_d° can be estimated from the experimental data and eqs 2−8. For the case in which α, b^w, and b^{org} are 0.5, 0.4 and 0.6, respectively, $k_a^{w\,\circ}$ and $k_a^{org\,\circ}$ can be estimated of the order of 10^9-10^{10} cm^3 mol^{-1} s^{-1}. On the other hand, $k_a^{org\,\circ}$ was evaluated as ca. 3×10^{-2} s^{-1} while the desorption parameter from the aqueous side was relatively larger, i.e., $k_a^{w\,\circ} \sim 1$ s^{-1}. The experimental values obtained for k_a° can be compared with those expected for a diffusion-controlled adsorption. For instance, the change in the interfacial concentration (Γ_i) determined by diffusion to an adsorption plane can be simply estimated from the Einstein−Smoluchowski expression,

$$\frac{d\Gamma_i}{dt} = c_0 \nu_d = c_0 \frac{2D}{l} \tag{38}$$

where ν_d is the diffusion rate and l is the characteristic diffusion step length which can be taken of the order of the diameter of a water molecule, i.e., 150 pm, in the aqueous phase. Comparing eqs 1 and 38, it can be simply deduced that the rate constant for the diffusion controlled adsorption in the low coverage limit is given by

$$k_a^{diff} = 2D/l\Gamma_s \tag{39}$$

For a saturated interfacial concentration of the order of 10^{-10} mol cm^{-2} and common values of diffusion coefficients, k_a^{diff} can be evaluated to be in the range of 10^{13} mol^{-1} cm^3 s^{-1}. The relationship between k_a^{diff} and k_a° is determined by the activation energy for the adsorption process (ΔG_a^{act}).

$$k_a^\circ = k_a^{diff} \exp(-\Delta G_a^{act}/RT) \tag{40}$$

On the other hand, desorption inherently involves an activation energy (ΔG_d^{act}) in order to overcome the energy well associated with the adsorbed state. Similarly to eq 40, k_d° can be expressed in terms of ΔG_d^{act} by

$$k_d^\circ = \nu_f \exp(-\Delta G_d^{act}/RT) \tag{41}$$

where ν_f corresponds to the characteristic frequency of nuclear motion of species confined to a surface, typically 10^{14} s^{-1}. Assuming that ΔG_d^{act} is of the order of the Gibbs energy of adsorption determined for a variety of specifically adsorbed species, i.e., −40 kJ mol^{-1},[19,21,26,45] k_d° is evaluated as ca. 10^7 s^{-1}. Estimations of the activation energies employing eqs 39 and 40 results in values of the order of 20 kJ mol^{-1} for the adsorption process, while the apparent ΔG_d^{act} lies in the region of 70−90 kJ mol^{-1}. Although further experimentation is required to confirm these initial findings, the high activation energies could reflect distortion in the porphyrin structure and/or reorganization of the solvation shell during the adsorption process. These effects could also be responsible for the preferential orientation of the adsorbed molecule at the interface.[29]

The present analysis provides an unprecedented approach to the dynamics of ionic adsorption at a polarized ITIES. Key aspects remains to be addressed thoroughly, namely the potential distribution across the interface. Our model is based on a rather simple dependence of the adsorption rate constant on the Galvani potential difference (eqs 2−5). Although this approach may be valid for small potential perturbation, substantial deviation may occur over a large potential range. This is evidenced by the fact that the potential dependence of the PMF response displayed in Figure 8 could not be closely reproduced by the parameters obtained from the frequency response studies. In this respect, a relevant aspect ignored in this model is the local potential perturbation induced by specifically adsorbed ions. Recently, Frank and Schmickler have evaluated this effect on the dynamics of heterogeneous electron transfer by lattice-gas modeling.[46] It is clear that a more comprehensive study is required in order to gain further understanding on the potential distribution across the interface and its effect on adsorption dynamics.

5. Conclusions

The ion transfer and adsorption behaviors of fluorescent species at polarized liquid|liquid interfaces could be effectively studied by the frequency dependence analysis of the PMF responses. In the $Ru(bpy)_3$ system, the perturbation of the interfacial concentration manifested itself in a fashion similar to the faradaic impedance for a quasi-reversible ion transfer in the complex plane. For kinetically controlled adsorption processes, the complex representation of the PMF response described a semicircle in which the maximum of the imaginary component is determined by the adsorption and desorption rate constants. Furthermore, the location of the adsorption plane with respect to the interface can be unambiguously determined by the phase shift of the PMF responses. In the ZnTMPyP system, the adsorption responses observed at either side of the formal transfer potential exhibited the basic features associated with kinetically controlled adsorption process. The 180° phase shift between both responses as well as the fluorescence quenching in the presence of TCNQ effectively confirmed that the adsorption takes place at both sides of the interface. The adsorption kinetics of $ZnTMPyP^{4+}$ was determined in the frequency range below 100 Hz. It is believed that slow dynamics are determined by a high activation energy related to changes in the molecular structure originating from specific interfacial interactions. These interactions could also be connected to the preferential orientation of the adsorbed species at the interface.

Finally, despite that a phenomenological model appears to overestimate the potential dependence of the PMF responses, some relevant aspects were disclosed. It was observed that the adsorption takes place in the aqueous side of the interface was

weakly dependent on the applied potential in comparison to the organic side. At a first glance, this result agrees with the potential distribution described by the modified Verwey−Niessen model. However, the PMF responses for the adsorption at the aqueous side suggested that the effective charge number of the adsorbed species is somewhat lower than +4. We believe that these studies can also deliver an effective approach to study the ion-pair formation as well as local potentials across the interface.

Acknowledgment. This work is supported by the Fond Nationale Suisse de la Recherche Scientifique (20-055692.98/1). H.N. gratefully acknowledges the JSPS Research Fellowships for Young Scientists and Grant-in-Aid for JSPS Fellows (1090 and 01479) from the Ministry of Education, Science, Sports and Culture, Japan. The authors are grateful for the enlightening discussions with Prof. W. Schmickler (University of Ulm), Prof. Z. Samec (J. Heyrovský Institute of Physical Chemistry) and Prof. K. Nakatani (University of Tsukuba). The authors are also indebted to the contributions by Dr. H. Jensen and Dr. A. Piron, as well as to the technical assistance by V. Devaud. The Laboratoire d'Electrochimie is part of the European Network ODRELLI (Organization, Dynamics and Reactivity at Liquid|Liquid Interfaces).

References and Notes

(1) Corn, R. M.; Higgins, D. A. *Chem. Rev.* **1994**, *94*, 107−125.
(2) Eisenthal, K. B. *Chem. Rev.* **1996**, *96*, 1343−1360.
(3) Brevet, P.-F.; Girault, H. H. In *Liquid|Liquid Interfaces, Theory and Methods*; Volkov, A. G., Deamer, D. W., Eds.; CRC Press: Boca Raton, FL, 1996; p Chapter 6.
(4) Tsukahara, S.; Yamada, Y.; Watarai, H. *Langmuir* **2000**, *16*, 6787−6794.
(5) Saitoh, Y.; Watarai, H. *Bull. Chem. Soc. Jpn.* **1997**, *70*, 351−358.
(6) Ishizaka, S.; Nakatani, K.; Habuchi, S.; Kitamura, N. *Anal. Chem.* **1999**, *71*, 419−426.
(7) Ishizaka, S.; Habuchi, S.; Kim, H. B.; Kitamura, N. *Anal. Chem.* **1999**, *71*, 3382−3389.
(8) Schweighofer, K. J.; Benjamin, I. *J. Electroanal. Chem.* **1995**, *391*, 1−10.
(9) Benjamin, I. *Chem. Rev.* **1996**, *96*, 1449−1475.
(10) Benjamin, I. *Annu. Rev. Phys. Chem.* **1997**, *48*, 407−451.
(11) Schmickler, W. *J. Electroanal. Chem.* **1997**, *428*, 123−127.
(12) Schmickler, W. *J. Electroanal. Chem.* **1997**, *426*, 5−9.
(13) Girault, H. H. *Electrochim. Acta* **1987**, *32*, 383−385.
(14) Girault, H. H.; Schiffrin, D. J. In *Electroanalytical Chemistry*; Bard, A. J., Ed.; Marcel Dekker: New York, 1989; Vol. 15, pp 1−141.
(15) Strutwolf, J.; Barker, A. L.; Gonsalves, M.; Caruana, D. J.; Unwin, P. R.; Williams, D. E.; Webster, J. R. P. *J. Electroanal. Chem.* **2000**, *483*, 163−173.
(16) Naujok, R. R.; Higgins, D. A.; Hanken, D. G.; Corn, R. M. *J. Chem. Soc., Faraday Trans.* **1995**, *91*, 1411−1420.
(17) Naujok, R. R.; Paul, H. J.; Corn, R. M. *J. Phys. Chem.* **1996**, *100*, 10497−10507.
(18) Conboy, J. C.; Richmond, G. L. *J. Phys. Chem. B* **1997**, *101*, 983−990.
(19) Piron, A.; Brevet, P.-F.; Girault, H. H. *J. Electroanal. Chem.* **2000**, *483*, 29−36.
(20) Rinuy, J.; Piron, A.; Brevet, P.-F.; Blanchard-Desce, M.; Girault, H. H. *Chem.−Eur. J.* **2000**, *6*, 3434−3441.
(21) Higgins, D. A.; Corn, R. M. *J. Phys. Chem.* **1993**, *97*, 489−493.
(22) Samec, Z.; Marecek, V.; Homolka, D. *Faraday Discuss. Chem. Soc.* **1984**, 197−208.
(23) Samec, Z.; Marecek, V.; Homolka, D. *J. Electroanal. Chem.* **1985**, *187*, 31−51.
(24) Girault, H. H.; Schiffrin, D. J. *J. Electroanal. Chem.* **1985**, *195*, 213−227.
(25) Fermín, D. J.; Duong, H. D.; Ding, Z. F.; Brevet, P.-F.; Girault, H. H. *Phys. Chem. Chem. Phys.* **1999**, *1*, 1461−1467.
(26) Fermín, D. J.; Ding, Z. F.; Duong, H. D.; Brevet, P.-F.; Girault, H. H. *J. Phys. Chem. B* **1998**, *102*, 10334−10341.
(27) Jensen, H.; Kakkassery, J. J.; Nagatani, H.; Fermín, D. J.; Girault, H. H. *J. Am. Chem. Soc.* **2000**, *122*, 10943−10948.
(28) Jensen, H.; Fermín, D. J.; Girault, H. H. *Phys. Chem. Chem. Phys.* **2001**, *3*, 2503−2508.
(29) Nagatani, H.; Iglesias, R. A.; Fermín, D. J.; Brevet, P.-F.; Girault, H. H. *J. Phys. Chem. B* **2000**, *104*, 6869−6876.
(30) Nagatani, H.; Piron, A.; Brevet, P.-F.; Fermín, D. J.; Girault, H. H. In preparation.
(31) Samec, Z. *Chem. Rev.* **1988**, *88*, 617−632.
(32) Kakiuchi, T. *J. Electroanal. Chem.* **2001**, *496*, 137−142.
(33) Markin, V. S.; Volkov, A. G. In *Liquid−Liquid Interfaces, Theory and Methods*; Volkov, A. G., Deamer, D. W., Eds.; CRC Press: Boca Raton, FL, 1996; Chapter 4.
(34) Kakiuchi, T.; Takasu, Y. *Anal. Chem.* **1994**, *66*, 1853−1859.
(35) Osakai, T.; Kakutani, T.; Senda, M. *Bull. Chem. Soc. Jpn.* **1985**, *58*, 2626−2633.
(36) Osakai, T.; Kakutani, T.; Senda, M. *Bull. Chem. Soc. Jpn.* **1984**, *57*, 370−376.
(37) Wandlowski, T.; Marecek, V.; Samec, Z. *J. Electroanal. Chem.* **1988**, *242*, 291−302.
(38) Fermín, D. J.; Ding, Z.; Brevet, P.-F.; Girault, H. H. *J. Electroanal. Chem.* **1998**, *447*, 125−133.
(39) Sluyters-Rehbach, M.; Sluyters, J. H. In *Comprehensive Treatise of Electrochemistry*; Yeager, E., Bockris, J. O. M., Conway, B. E., Sarangapani, S., Eds.; Plenum Press: New York, 1984; Vol. 9.
(40) Senda, M.; Delahay, P. *J. Phys. Chem.* **1961**, *65*, 1580−1588.
(41) Sluyters-Rehbach, M.; Timmer, B.; Sluyters, J. H. *Recl. Trav. Chim. Pays-Bas* **1963**, *82*, 553−564.
(42) Delahay, P. *J. Phys. Chem.* **1966**, *70*, 2373−2379.
(43) Kakiuchi, T.; Takasu, Y. *J. Phys. Chem. B* **1997**, *101*, 5963−5968.
(44) Kalyanasundaram, K. *Photochemistry of Polypyridine and Porphyrin Complexes*; Academic Press: London, 1992.
(45) Wandlowski, T.; Marecek, V.; Samec, Z. *J. Electroanal. Chem.* **1988**, *242*, 277−290.
(46) Frank, S.; Schmickler, W., *J. Electroanal. Chem.* **2001**, *500*, 491−497.